01 Sep 1975

Compliant Wall Surface Motion and its Effect on the Structure of a Turbulent Boundary Layer

R. L. Ash

D. M. Bushnell

L. M. Weinstein

R. Balasubramanian

COMPLIANT WALL SURFACE MOTION AND ITS EFFECT ON THE STRUCTURE OF A TURBULENT BOUNDARY LAYER

Robert L. Ash
School of Engineering
Old Dominion University
Norfolk, Virginia 23508

Dennis M. Bushnell and Leonard M. Weinstein
NASA Langley Research Center
Hampton, Virginia 23665

R. Balasubramanian
Old Dominion University
Research Foundation
Norfolk, Virginia 23508

ABSTRACT

The status of the continuing compliant wall drag reduction research at NASA-Langley Research Center is discussed. Preliminary surface motion calculations are reported along with compliant surface design concepts and their numerical models. A compliant drag reduction theory based on stabilizing the turbulent substructure is proposed and previous experiments have been examined relative to that theory. Results of recent low speed compliant surface experiments have been reported which include initial attempts to measure local compliant surface motion.

1. INTRODUCTION

Ffowcs-Williams (1964) suggested how the motion of a flexible surface beneath a fully turbulent boundary layer might reduce the skin friction drag. His analysis was based on the earlier work of Kramer (1965) who was concerned primarily with the ability of a compliant surface to delay boundary layer transition. Kramer's experiments were not closely controlled and only recently have successful transition delay experiments been reported (Babenko, 1973). Between 1966 and 1969, E.F. Blick and his students at the University of Oklahoma reported significant drag reduction measurements beneath fully turbulent boundary layers. Most of their work is summarized by Blick, et al. (1969). Their work, as well as the limited number of additional successful experiments, have been analyzed by Ash (1974) and Fischer, et al. (1975). The fact that more unsuccessful experiments are found in the literature than successful experiments is due primarily to the complexity of the problem. Specifically, the problem is how a pressure driven surface motion can interact with and modify a turbulent flow structure. The turbulent substructure has only recently been identified and is still not completely understood. Also, no detailed surface motion measurements have been obtained during successful drag reduction experiments. Therefore, quantitative theoretical models of the phenomenon have not been possible and, as a result, successful compliant wall experiments have been very difficult to reproduce.

The lack of surface motion measurements has created a severe problem in systematically analyzing the compliant wall drag reduction mechanism. Obviously, the surface motion is responsible for alteration of the turbulent structure, but until the actual surface motion is known neither the type of surface motion required nor the effect of the motion on the turbulent structure can be positively identified. The present work has attacked the surface motion problem from three directions. First, a numerical capability is being developed which will permit design of compliant structures with specific types of surface motion. Second, theoretical models are being conceptualized which identify types of fluid-surface interactions and provide input for the surface design. Third, surface measurement capabilities are being developed which can monitor surface motion during successful experiments as well as verify the numerical calculations and permit improved modeling. None of the three phases is complete at this time.

This status report discusses the progress made in all three aspects of the analysis. The structural calculations are presented first because they are relevant to the overall fluid-structure interaction problem and not just compliant wall drag reduction. Surface motion analysis has proceeded from natural frequency or eigenvalue calculations to transient motion predictions for

a single convected pressure fluctuation. The present status of that work is discussed and future directions identified. The most recent theoretical model has been presented along with the logic behind its formulation. Following that model, a retrospective examination of possible surface motions during previous successful experiments has been used to evaluate the proposed model. Finally, the current status of the experimental program has been discussed and results of a preliminary surface motion study are presented.

2. DYNAMIC STRUCTURAL CHARACTERISTICS OF COMPLIANT SURFACE MOTION

Types of Surface Motion

Past experiments indicate that surface motion must be closely controlled in order to alter favorably the structure of the turbulent boundary layer. Control of passive systems driven by turbulent wall pressure fluctuations is extremely difficult and presently can only be attempted through general design concepts rather than strict actual control. Design concept control means an ability to control in some sense the amplitude, wave length, wave speed, and wave form of the surface motion. Two passive design concepts have been identified and will be discussed in some detail. A third "active wall" concept which is considered of less practical importance will also be discussed later because of its relationship with passive design requirements.

The two passive design concepts have been classified as resonant and flow triggered. A resonant motion is essentially a controlled panel flutter state. Resonating surfaces filter from the turbulent spectrum those wall pressure fluctuation frequencies which are compatible with their own characteristic vibration frequencies. As a result, nodal standing wave patterns can be excited and sustained on the surface. By contrast, a flow triggered surface is a truly compliant surface. Unlike the resonant wall, the flow triggered wall motion is controlled by the instantaneous local pressure fluctuations. In general, the flow triggered wall cannot respond instantly to the pressure fluctuations because of its mass and damping, hence there will be some phase lag between the driving pressure force and the local surface response. In air, flow triggered surfaces are considered unlikely because of the mismatch between air density and the density of solid materials.

Design Concepts

An additional constraint on design is the desirability of creating a drag reducing surface which will be durable enough to have practical applications (for example, on a CTOL airplane fuselage). As a consequence, the present effort has not used extensively the membrane-like surfaces employed successfully by Blick, et al. (1969), since they are too fragile to be used on transportation vehicles. However, for purposes of discussion, the wealth of information available on membranes has been used to assess the effects of surface motion and damping on the skin friction reduction.

Four primary structural design configurations have been identified and are shown in Figure 1. (a) Membrane surfaces have been the subject of many previous investigations. (b) Rigidly backed elastic slabs have been tested with little success due to static standing wave patterns which are ultimately set up on the surface (in agreement with the previous work of Nonweiler, 1963 and Hansen and Hunston, 1974). (c) Laminated structures have been tested primarily by the Langley Research Center group and have shown some promise as viable drag reducing surfaces. (d) Periodic structures have only recently been considered and are still in preliminary design stages. As mentioned previously, the paucity of experimentally measured surface motion data has forced design concepts to rely heavily on numerically calculated surface motions. The various calculation techniques employed will be discussed subsequently.

Restricting attention to resonant wall motions, general vibration features of the four design concepts (fig. 1) can be discussed without involving numerical details. An attempt has been made to categorize the design configurations as either broad band or narrow band response systems. A broad band response is defined as a system where resonant vibration modes are discretely spaced, beginning from the fundamental mode, in some uniform manner. Narrow band response means large numbers of resonant vibration frequencies are concentrated in narrow frequency bands followed by a frequency interval with no characteristic resonant frequencies. Such a classification is important here because it gives an indication of the certainty of having a measurable contribution from a particular frequency component in the surface motion (broad band is less certain than narrow band). Membranes over deep cavities and simple elastic slabs are categorized as broad band systems, while the laminated and periodic structures can be considered narrow band. Both types of systems have advantages and disadvantages. Broad band systems allow more control over wave shape and wave speed because there are fewer resonant vibration modes over a particular frequency range. However, if little damping is present, several distinctly different

resonant vibration patterns (with different nominal frequencies) can be excited by the same turbulent boundary layer. The narrow band systems offer frequency control because the coupled systems force large numbers of vibration modes to be crowded around a single frequency. However, the crowding removes nearly all control over wave shape and speed.

A fifth configuration has been identified which is a hybrid of the membrane with cavity and the laminated structure shown in Figure 1. As suggested by Ash (1974), there may have been a small air gap between the membrane and elastic substrate in the experiments of Blick, et al. (1969). The influence of a small air gap on the membrane surface motion has been modeled numerically and those results help explain why more recent experiments by McAlister and Wynn (1974) did not reproduce the measurements of Blick, et al. (1969) as well as how temperature variations could have affected the experiments of Fischer, et al. (1975). Analysis of that configuration (membrane with narrow air gap) is presented at the end of the numerical calculations.

Numerical Calculations

With the exception of simple membranes and simplified elastic slab models, all structural calculations have required numerical analysis. The development of realistic dynamic surface predictions has proceeded from vibration (eigenvalue) analysis through calculation of the transient motion produced by a single convected pressure fluctuation. Development of a simulated turbulent wall pressure has begun but will not be discussed here.

Eigenvalue or natural frequency calculations provide useful preliminary information because they allow a particular design concept to be identified according to its vibration frequencies thereby indicating wide band or narrow band response characteristics. However, they do not indicate either the amplitude or character of a turbulent wall pressure driven surface motion. Rather than present a wide range of eigenvalue calculations, a standard compliant model configuration has been employed. Hence, a comparison of vibration mode distributions can be made for the four primary design concepts using the same materials and dimensions. The same standard model will also be used in the dynamic calculations.

Standard Model Properties and Dimensions. Unless otherwise noted, a standard membrane and elastic substrate have been used in this analysis. The standard model has shown a consistent 10 to 15 percent skin friction reduction. The length in the flow direction (L) is 1.372 m and the width (W) is 0.457 m. When employing a membrane or skin, mylar with density (ρ_s) 1394/Kg/m^3 and thickness (h) 0.025 mm is used. Applied tensions in the flow (T_x) and cross-stream (T_z) directions are assumed equal ($T_x = T_z = T$) and a value of 175 N/m is used. The elastic substrate is compressed polyurethane foam (Scottfelt) with a nominal porosity of 35 pores per cm. Its modulus of elasticity (E_f) is 1.38 N/cm^2 and density (ρ_f) is 115 Kg/m^3. The assumed thickness of the substrate (H) is 6.35 mm.

Eigenvalue Calculations. Membrane: Eigenvalues for rectangular membranes can be calculated directly from the algebraic expression:

$$f_{n,m} = \frac{1}{2}\left(\frac{n^2T_x/L^2 + m^2T_z/W^2}{\rho_s h}\right)^{1/2} \qquad (1)$$

The actual vibration frequencies will be shifted from the calculated values by damping, but since damping varies with the particular environment, the undamped values are used for reference. The first ten eigenvalues for the standard membrane are given in Table 1.

Elastic Slab: A wide variety of vibration frequencies can be calculated for a simple elastic slab. From Kolsky (1953), there are three distinct types of stress waves which can be propagated along the surface--dilatational, shear, and surface (Rayleigh) waves--and any or all of them may be important. However, in this work a simplistic elastic spring calculation has been used assuming the slab experiences only planar vibrations. Under those conditions the eigenvalues or natural frequencies are given by:

$$f_n = \frac{n}{2H}\left(\frac{E_f}{\rho_f}\right)^{1/2} \qquad (2)$$

The first ten vibration frequencies for the standard elastic substrate are given in Table 1.

Laminated Structure: An approximate analytic model and a purely numerical model were used to calculate the eigenvalues for the laminated structure. Both models have neglected the effect of bonding material. Although not included here, the influence of bonding material, which can be important, has been studied to a limited extent by lumping its properties and thickness with either membrane or the substrate depending on which was most similar.

If the membrane is modeled as a pre-stressed plate of infinite extent and the substrate is modeled as a continuous distribution of independently acting vertical springs, the natural radian frequencies ($\omega_{m,n}$) are solutions of the transcendental equation:

$$(\rho_f E_f)^{1/2}\,\omega_{m,n}\cot\left[(\rho_f/E_f)^{1/2}\omega_{m,n}H\right] + \left[\left(\frac{n\pi}{L}\right)^2+\left(\frac{m\pi}{W}\right)^2\right]\left\{T + D\left[\left(\frac{n\pi}{L}\right)^2+\left(\frac{m\pi}{W}\right)^2\right]\right\} \quad (3)$$

$$= \rho_f h\,\omega_{m,n}^2$$

where D is the plate stiffness given by:

$$D = E_s h^3/[12(1-\nu_s^2)]\ ,$$

and ν_s is Poisson's ratio for the skin ($\nu_s = 0.3$ for mylar). The first ten eigenvalues for the standard model have been calculated from Equation (3) and are given in Table 1.

The other, more complete model included boundary conditions at the finite edges and allowed the substrate to behave as an elastic slab rather than the continuous elastic spring model used for the elastic foundation, used in Equation (3). That model was solved by numerical methods. Three structural models were used to calculate numerically the eigenvalues for the laminated structure. All three were simulated by a finite element NASTRAN (MacNeal, 1972) program. The three-dimensionality of the structure was incorporated in two of these models and a two-dimensional approximation was used in the third. Details of the models are presented in the next section. The two-dimensional approximation permitted an increase in the number of elements (or nodes), thereby improving the resolution. The excellent agreement between the different models suggested that the two-dimensional model was adequate for the present numerical simulation. Results of the two-dimensional eigenvalue calculations are given in Table 1.

An important result of both the NASTRAN calculations and Equation (3) is that the applied skin tension had a very small effect on the eigenvalues for the laminated or sandwich surfaces.

Periodic Structure: By design, periodic structures utilize repeating structural elements to control vibration frequency. As a consequence, the number of vibration modes in a particular frequency band are controlled by the number of repeated elements. Since only preliminary design considerations have been given to that structure, the number of repeated elements has not been specified. However, as a computational sample, four structural cycles have been included in this study. The standard skin is assumed anchored to 1-mm-wide transverse aluminum ribs. The spacing between the ribs was 1.5 mm and that region was assumed filled with the 35 pores per cm polyurethane foam. No algebraic expression is available for that system and the two-dimensional model of the structure was analyzed using the NASTRAN program to calculate the eigenvalues in Table 1. Because of the previously mentioned dependence on the number of structural cycles, the first ten calculated eigenvalues are not representative of the desired structure. However, they do show where frequency bands will occur as indicated in the table.

Dynamic Surface Motion Calculations. In order to isolate the compliant wall effect, either a simple wave motion must be identified from turbulence theory and designed into a structure or a simulated surface motion predicted for a particular compliant model must be employed in the theory. Logically, the surface motion should be coupled to any turbulent simulation. All of these approaches require accurate numerical prediction techniques and the transient methods discussed here appear capable ultimately of meeting all requirements.

Recently, Leehey and Davies (1975) have published a theoretical analysis of the motion of a membrane driven by a turbulent pressure spectrum. That work does not present instantaneous surface predictions, but rather cross spectral data. Furthermore, due to the approximations employed, it appears to be limited to long narrow membranes. However, it does represent an alternate approach to the direct numerical simulation techniques which will ultimately be used in this investigation.

Calculations for membrane motions will be employed only where they are related to the small air gap problem. Further calculations will be made when the turbulent pressure simulation program has been developed. No dynamic calculations have been made for the periodic structure because the preliminary design-eigenvalue analysis is not complete.

Since a simple elastic slab is a special case of the laminated structure, details of the laminated structure analysis represent both cases. (Actually, the periodic structure is also a modified laminated structure.) The work reported here has concentrated on calculating surface motions resulting from a single convected pressure fluctuation, because of its application to the turbulent pressure simulation. Since two-dimensional simulations are more economical, they have been studied more extensively. The pressure fluctuation has been modeled initially as a single

cycle plane sine wave. Both two- and three-dimensional structures have been analyzed, but the sizes of the present three-dimensional elements (nearly 20 cm long) are too large to yield meaningful surface motions.

The three structural models mentioned in the eigenvalue calculations were all considered for use in dynamic simulations, but the finite three-dimensional "plate on an elastic foundation model" has not been used because the crudeness of the approximations was not justified. Choice of element combinations will affect accuracy, reliability, and efficiency in the dynamic numerical simulations. Interested users should consult the theoretical NASTRAN manual (MacNeal, 1972) for details, but the three element combinations (including the finite plate on an elastic foundation) are listed below as model (1), (2), and (3). The models are listed here in descending order based on required computer time (most time required first).

Model (1) Fully three-dimensional system. Skin is modeled as thin plate elements (CQUAD 1). Substrate is modeled as full three-dimensional elements (CHEXA2). No provision is made for offset between thin plate grid points and the surface grid points of the three-dimensional elements, but the thickness of the plate (skin) is extremely small and hence the error introduced is small.

Model (2) Finite plate on an elastic foundation. Skin is modeled as thin plate elements (CQUAD 1). Substrate is modeled as a collection of spring-mass elements calculated from a static three-dimensional analysis using isoparametric elements (CIHEX3).

Model (3) Two-dimensional model. Skin is modeled as bar elements (CBAR). Membrane analogy has been used to model exactly the substrate as membrane elements (CQDMEM1). Offsets were used for exact matching.

Because different size elements have been used in the three-dimensional transient calculations than in the two-dimensional calculations, a direct comparison cannot be made. However, the two-dimensional model (3) costs about one-fourth as much to run as the three-dimensional model (1) and overestimates surface motion by up to 20 percent. The overestimation problem at this stage is considered less important than the cost and consequently the two-dimensional results will be presented here (without dimensions) because of their higher resolution.

The NASTRAN program satisfactorily performed all transient calculations for the element models described. Direct transient calculations were generated using the Newmark (1959) β method of time integration which is unconditionally stable. However, in order to assure high resolution of the surface motion, time steps were selected which are less than one-tenth of the period of the highest frequency of interest.

Viscous structural damping was introduced in the calculations by constructing complex stiffness (modulus of elasticity can be represented as a complex number for viscoelastic materials). The NASTRAN representation for damping forces the damping coefficient β to vary with frequency according to:

$$\beta(\omega) = \frac{\beta_o}{\omega_o}\omega \qquad (4)$$

where ω is the radian frequency. Arbitrarily setting $\beta_o = 1$, proper choice of ω_o permits realistic simulation of viscoelastic damping.

As mentioned earlier, the standard laminated model has produced a fairly consistent 10 to 15 percent Reynolds stress reduction during wind tunnel tests with free stream velocities in the 60 m/sec range. Pressure fluctuations are known to convect downstream with velocities of about 0.8 U_∞. Consequently, a convection velocity of 43 m/sec (U_∞ = 54 m/sec) has been used in the pressure fluctuation calculations. Furthermore, based on the free stream velocity and boundary layer thickness, the nominal peak in the turbulent wall pressure spectrum was 300 Hz. The energy content has dropped significantly for pressure fluctuations outside the 50 to 500 Hz range and therefore only that range was considered. Data indicate that mylar is nearly elastic and preliminary experiments on the Scottfelt foam indicate the damping coefficient can be approximated between ω_o values of 1885 (high damping) and 94,250 rad/sec (low damping).

Using these data, transient surface motion histories have been calculated over the indicated ranges of frequency and damping. No startling effects were observed, as indicated by representative surface histories for the lowest damping cases with convected pressure frequencies of 300 and 500 Hz (shown in Figure 2). The 500 Hz motion decays more rapidly due to the 70 percent larger damping coefficient. Damping will be highly frequency dependent for the foam sub-

strates employed in the experiments, but whether Equation (4) represents a realistic distribution is not presently known.

In order to extract response characteristics from the transient data, a Fast Fourier Transform (FFT) has been employed. Since damping makes the surface response aperiodic (the amplitude decays with time, creating an apparent low frequency component), the spectral analysis will be misleading at low frequencies. Using the lightly damped surface motion for a 300 Hz pressure fluctuation shown in Figure 2, the spectrum shown in Figure 3 results. Due to the nature of the single sine wave driving force, a simplified Duhamel integral analysis shows that the combination of the driving force frequency (300 Hz) and the fundamental vibration frequency (453 Hz) results in an apparent frequency of 377 Hz [(300 + 453)/2], along with a beat frequency of 77 Hz [(453 - 300)/2]. The strong dominance of the fundamental vibration mode, as indicated by the spectrum, is not surprising because of the nearness of the forcing frequency to the fundamental frequency.

Several simplistic methods have been employed to estimate the group velocity of surface waves. Group velocity is the conventional apparent velocity of a wave packet. One approach was to impulsively load a point on the surface of the model and measure the time required for an amplitude peak to pass between successive network points. Conceptually, the method seemed adequate but because of the quasi-steady calculation procedure used in the NASTRAN program, that approach cannot be used for these systems. A second method has attempted to use the spatial amplitude distributions at two successive time steps as shown in Figure 4. However, the assumed convection speed dominates during the time when the single pressure pulse is over the surface and thereafter waves are travelling in both directions, making this approach inadequate. Currently, a two-point autocorrelation procedure is being investigated, but no reliable group velocity estimates have been obtained at this time.

The discussion presented thus far has indicated design tools which are being used to develop compliant wall concepts. The laminated structural model has been used primarily because it has been studied more extensively than the others and our experiments have shown it may be capable of some drag reduction. Unfortunately, at present neither the resolution for the model nor the simulations are sufficiently accurate to yield quantitative data for our theoretical models. Neither problem has been the result of computer limitations, although there are limitations on the full three-dimensional simulation. The present limitations have been self-imposed while the necessary numerical skills and models were developed.

Finite difference methods can appropriately be used in transient membrane problems and the nonlinear problem created by an air gap has been examined using that method.

Analysis of a Membrane Over a Small Gap. The conceptual compliant wall drag reduction theory which is presented in the next section indicates a requirement for very short wavelengths for effective fluid-surface interactions. If that inference is correct, there is some question as to how a large membrane could be excited in those vibration modes. One possible mechanism for producing that type of surface motion may have been the small air gap which probably existed between the membrane and substrate in Blick's (1969) experiments (the skin and substrate were not attached). When the membrane contacts the substrate, the substrate resists further downward motion and there would be a tendency for the surface to "chop" the long wavelength motions into higher frequency short wavelength motions. A preliminary study on the influence of a small air gap is presented here. As a starting point, a membrane over a deep cavity is modeled, then the equations are modified to include the effect of a small gap.

The governing equation for unsteady vertical displacements of a rectangular membrane with uniform tension is:

$$\frac{\partial^2 \zeta}{\partial x^2} + \frac{\partial^2 \zeta}{\partial z^2} - \frac{P(x,z,t)}{T} = \frac{1}{C^2}\frac{\partial^2 \zeta}{\partial t^2} + \frac{\beta}{T}\frac{\partial \zeta}{\partial t} \qquad (5)$$

where $C = (T/\rho_s h)^{1/2}$ is the wave speed. If $P(x,z,t)$ is an impulsive point load at $t = 0$,

$$P(x,z,t) = P_0\, \delta(x - x_0)\, \delta(z - z_0)\, \delta(t - 0) ,$$

equation (5) has the exact solution

$$\zeta(x,z,t) = \frac{-4P_0 c}{LWT} \sum_{m,n=1}^{\infty}\sum \sin\frac{n\pi x_0}{L} \sin\frac{n\pi x}{L} \cdot \sin\frac{m\pi z_0}{W} \sin\frac{m\pi z}{W} \frac{\sin \Gamma_{mn} ct}{\Gamma_{mn}} \qquad (6)$$

where $\Gamma_{mn}^2 = (n\pi/L)^2 + (m\pi/W)^2 - c^2\beta^2/T^2$

The solution for the centerline response of the standard mylar membrane with an impulsive force applied at $\frac{L}{2}$, $\frac{W}{2}$, is shown in Figure 5a. A damping coefficient (β) of 1.6×10^{-4} N sec/m^3 has been assumed.

If the substrate beneath the gap is modeled as an elastic foundation, governing equation (5) can be modified to include its effect. The substrate then acts as an intermittently applied spring. That is, if the gap is γ_o thick, a spring reaction is introduced any time ζ is less than $-\gamma_o$. Employing the unit step function $U(\zeta_o - \zeta)$, which is zero when ζ is greater than ζ_o and unity when ζ is less than ζ_o, equation (5) can be rewritten as:

$$\frac{\partial^2 \zeta}{\partial x^2} + \frac{\partial^2 \zeta}{\partial z^2} - \frac{P}{T} = \frac{1}{C^2}\frac{\partial^2 \zeta}{\partial t^2} + \frac{\beta}{T}\frac{\partial \zeta}{\partial t} + (\zeta + \gamma_o)\frac{E_f}{HT} U(-\gamma_o - \zeta) \quad (7)$$

Unfortunately, even this simplified approximation has made the governing equations nonlinear and it was necessary to solve equation (7) using a finite difference method. Results for a 0.003 mm gap behind the same membrane modeled by equation (6) is shown in Figure 5b. In addition, the centerline motion produced by a convected 450 Hz pressure fluctuation for the same gap configuration are shown in Figure 5c.

Comparing Figures 5a and 5b, evidence of significantly larger high frequency contributions in the gap case are apparent. The nearly sinusoidal initial response for the gap has an apparent frequency of 1100 Hz while the first mode vibration frequency from Table 1 is 86 Hz. Although high frequency contributions are present in the simple membrane case, because of low damping, the low frequency contribution appears to dominate (amplitudes have been normalized for comparison). Because of the dominance of the applied pressure pulse, it is difficult to assess the influence of the gap in Figure 5c, although a high frequency component is certainly shown.

Of greater interest than frequency, at this point, is wavelength. An indication of wavelength can be obtained by investigating the instantaneous surface deflection. In order to achieve the resolution needed for small wavelength motion for the gap case, the influence of node size was investigated. A small 0.406 m by 0.125 m, 0.025-mm-thick mylar membrane was employed in order to use smaller node sizes. These calculations produced the instantaneous surface displacements shown in Figure 6. Figure 6a represents the analytic solution, Equation (6), with low air damping. Figures 6b and 6c are the numerically calculated air gap solutions showing the effect of node size. Figure 6b utilized a finite difference grid 2.5 cm by 2.5 cm, while Figure 6c shows the displacement on a finer 0.625 cm by 0.625 cm grid for the same two times. Significant differences in surface displacement distributions are shown in Figures 6b and 6c. The differences are due largely to the model employed for the elastic backing. That is, the nonlinear switch (unit step function) which activates the elastic spring model at each grid point strongly affects the surface motion depending on the size of the region over which each spring acts. The surface displacement distributions do suggest that wave speed is not significantly affected by a small air gap.

3. SUMMARY OF COMPLIANT STRUCTURE ANALYSIS

Based on structural dynamic calculations completed thus far, several general conclusions can be drawn. Eigenvalue calculations for the laminated systems have shown that very large numbers of resonant panel modes (characterized by the dimensions of the skin) have been crowded into a narrow frequency band. Furthermore, some of those panel vibration modes are capable of simultaneous resonance with the substructure. The simultaneous resonant modes are probably dominant in controlling surface motion, but smaller numerical elements will be required to verify that conclusion and guide this research toward designing specific vibrations into the structure. Due to the large number of eigenmodes, tighter design criteria must be established.

Very short wavelength (a few millimeters) motions cannot be detected in the numerical calculations--due to the size of the present computational elements. The homogeneous material model employed for the polyurethane foam will probably prevent short wavelength motions from occurring. However, the actual porosity of that foam (35 pores per centimeter) may invalidate the homogeneous material assumption and cause very small wavelength surface motions to be present. Examination of that possibility is continuing.

The small air gap calculations have shown that when a membrane skin is not bonded to its elastic substrate significant high frequency components of the surface motion exist. The size of the gap may be arbitrarily small and frequency shifting still occurs. The thickness of the gap should affect the wavelength of the surface motion but again the size of the nodes employed in the present network analysis are too large to pick up wavelength control.

Damping is a critical and, as yet, poorly estimated parameter in these calculations. The degree of internal damping in the laminated structures studied thus far appears to be excessive in that resonant surface vibrations are difficult to set up. Damping produced by the small air gap beneath the membrane may be as important as the gap in controlling the surface motion, but experiments are required to estimate its contribution.

The authors believe that structural design which utilizes rather abstract structural properties in a similarity analysis is inadequate in the study of the compliant wall effect. The parametric study of Babenko (1973) on transition delay is a recent example. These analyses give neither an indication of the actual surface motion occurring nor any clue on how the motions are excited. The turbulent pressure simulation approach which is currently being undertaken, along with detailed surface measurements, appears to be the only approach which can ultimately isolate the compliant wall effect.

Of the five design concepts considered, the elastic slab and membrane over a deep cavity do not appear to offer promise as viable drag reducing surfaces, although some drag reduction may occur over the membrane under very unique conditions (which will be discussed in the experimental section). The simultaneous resonance requirement for the laminated structure may be worth exploiting as a basis for control, but presently the number of simultaneous resonant modes identified for the current laminated structures is too large to permit any control. The membrane with a small air gap has been associated with the largest number of successful compliant wall experiments and should be continued primarily as a source for basic research into the compliant wall phenomenon. The gap appears to offer some frequency and wavelength control. The periodic structure offers unique structural advantages over the other four models because both frequency and wavelength can be controlled and durable surfaces can be constructed. Although a large number of vibration modes are crowded into a particular frequency band, they are associated with nearly identical wave forms between each support and they only represent the combinations of those waves which can occur over a large number of repeated elements. The last three concepts are under current investigation.

4. POSSIBLE COMPLIANT WALL DRAG REDUCTION MECHANISM

Flow Structure and "Events" in Turbulent Wall Boundary Layers

The existence of a "quasi-ordered" sequence of events in the near wall region of turbulent boundary layers is well documented (see Kline, et al., 1967; Corino and Brodkey, 1969; Blackwelder and Kaplan, 1971; Grass, 1971; Kim, et al., 1971; Willmarth and Lu, 1972; Wallace, et al., 1972; and Offen and Kline, 1974). Burton (1974) summarized the sequence of events usually observed (indicated schematically on Fig. 7). A relatively low speed streak (local velocity lower than its time average) occurs very near the wall, which undergoes further retardation. In the more severe of these retardations, a burst or ejection occurs. This burst and subsequent sweep provides the bulk of the Reynolds stress and turbulence production, while the flow between events and the pre-burst retardation region is relatively quiescent (low $\overline{u'v'}$). The "quasi-ordered" sequence of events appears to occur randomly in space and time. There is still considerable controversy as to the relationship between the retardation and the burst or ejection, but one possible interpretation is based upon the decreased stability of the retarded profile, i.e., the ejection or burst could be caused by an instability resulting from the inflected nature of the instantaneous retarded velocity profile.

Burton (1974) recently obtained experimental evidence indicating that the wall pressure fluctuations are imposed upon the near wall region by an "outer flow" ($y^+ \approx 400$). Furthermore, large adverse pressure gradient fluctuations imposed more or less randomly upon the near wall flow seem to trigger the quasi-ordered sequence of events. A sketch of this imposed adverse pressure gradient is given in Figure 8, along with an actual P vs. time pulse taken from Burton (1974).

To theoretically check Burton's observation of the connection between the retardation/burst cycle and an adverse pressure gradient imposed on the wall flow, a quasi-steady calculation was made of the near wall region using a typical pressure gradient as measured by Burton. The calculation procedure was a conventional non-similar finite difference boundary layer code (Bushnell and Beckwith, 1970). The outer edge of the calculation region was taken at $y^+ = 280$ ($u_e' = .6u_\infty$) for the boundary layer measurements in the low speed experiments of Fischer, et al. (1975) corresponding to $U_\infty = 61$ m/sec, $C_f = 2 \times 10^{-3}$, $\delta = 4.06$ cm. From typical experimental observations,

the initial instantaneous velocity profile was taken as a typical fully developed turbulent profile ($u^+ = y^+$ near wall, merging into the law of the wall at $y^+ \simeq 30$). The pressure gradient was imposed in the usual boundary layer fashion as an external boundary condition and was obtained from Burton's data (P vs. time) using Taylor's hypothesis, i.e.,

$$\frac{dP_e}{dx} \simeq - \frac{1}{u_{conv}} \frac{\Delta P}{\Delta t}$$

where $\Delta t \Rightarrow \Delta t^+ = 20$, $\Delta p \simeq 2.5 p'_{w,rms}$ (Fig. 8), and $u_{conv} = .8u_\infty$. Using a typical Δt^+ for the adverse dP/dx region of 20 and a convection speed of $.8u_\infty$ results in a Δx^+ for the retardation region of approximately 500, which is in the same range as indications from conditional sampling data.

Since the retardation period is relatively quiescent (low u'v') the fully developed turbulent shear stress model of Bushnell and Beckwith (1970) was decreased by a constant factor of the order of .1 (which is reasonable from the results of Kline, et al., 1967). The results from these calculations for the innermost region of the boundary layer are shown in Figure 9. It should be pointed out that since these calculations are quasi-steady and two-dimensional they should provide only a crude quantitative indication of the actual retardation. Results are shown for two values of $\overline{u'v'}/\overline{u'v'}_{rms}$, .05 and .1. If a factor of 1 were used (which would be incorrect based on the conditional sampling data) the imposed dP/dx measured by Burton would have only a negligible influence on the instantaneous profile. However, as seen from Figure 9, when the intermittent nature of the turbulent production is approximately accounted for (through the .05 or .1 factor), the "imposed dP/dx" affects the profile considerably within a reasonable Δx^+ range. In fact, the results shown in Figure 9 indicate (1) the extent of retardation typically measured ($\simeq$ 40 percent), and (2) the occurrence of an inflection point (but quite near the wall, at $y^+ \cong 2$). Based upon these calculations and Burton's measurements, it is perhaps reasonable to examine the possible influence of the motion from a "compliant wall" upon this "quasi-ordered," pressure gradient triggered, sequence of events.

Pressure Field Due to Compliant Wall Motion

In the simplest case the motion of a compliant wall consists of a traveling sine or cosine wave with a characteristic wave length and amplitude. For the low speed inviscid case the solution for the flow over a wavy wall is well known (Shapiro, 1954):

$$C_p = \frac{P - P_\infty}{\frac{1}{2}\rho_\infty U_\infty^2} = - \frac{4\pi}{\sigma} \frac{a}{\lambda} \cos 2\pi \left(\frac{x}{\lambda}\right) e^{-2\pi\sigma y/\lambda} \qquad (8)$$

where $\sigma = \sqrt{1 - m_\infty^2}$. This expression is composed of three components: an amplitude $\frac{4\pi}{\sigma}\frac{a}{\lambda}$; a modulation in phase with the wall motion $\cos 2\pi \left(\frac{x}{\lambda}\right)$; and an exponential decay away from the wall ($e^{-2\pi\sigma y/\lambda}$). For the low speed compliant wall case, and particularly for the present quasi-steady calculations, the decay term and σ are set equal to 1.

For the compliant wall case the amplitude of the wall motion must be small compared to the boundary thickness and, therefore, we do not have the inviscid case noted above (see Kendall, 1970; Yu, et al., 1973; Inger and Williams, 1972; Rogers, 1974; Yu and Hsu, 1971; Shemdin and Hsu, 1967). Due partly to the lower effective dynamic pressure within the boundary layer, and the smoothing effect of the displacement thickness, there is considerable diminution in the ΔP caused by a wavy wall in a thick turbulent boundary layer compared to the prediction of Equation (8). Also, a phase shift occurs between the wall motion and the induced pressure field. The phase shift is not important to the current "zeroth order" calculations, but could become critical in later, more detailed, compliant wall stability theory calculations. As stated, the amplitude of the wall motion for the compliant wall case is the order of the sublayer thickness, whereas in most of the "wavy wall" experiments the wall motion amplitude was large enough to possibly create an effective roughness, which could alter the magnitude of the wall induced pressure. The experiments of Kendall (1970) are probably closest to the compliant wall case and these data are shown in Figure 10. The measured C_p values are normalized by the inviscid C_{po} from Equation (8).

For the compliant wall calculations described in the next section a value of C_p/C_{po} of .1 was used. This value was taken from Figure 10 by extrapolating to $h^+ < 10$ and assuming that $C/u_\infty \simeq .25$. Although the influence of C was not directly included in the quasi-steady calculation described next, an attempt was made to account for a small positive C by using the .1 value for C_p/C_{po} (rather than the .2 for $C \simeq 0$ from Fig. 10a).

Possible Compliant Wall Turbulent Drag Reduction Mechanism

A compliant wall probably alters the "turbulent events" which are nearest the wall, therefore, the influence of the compliant wall pressure field on the retardation process was computed using the same calculation procedure employed to obtain the results shown in Figure 9. It should be noted that this calculation procedure has employed assumptions which may affect key elements in the compliant wall phenomenon:

(a) Procedure is quasi-steady rather than time-dependent.

(b) Does not include velocity field induced by the wall motion.

(c) The pressure field is a simple linear superposition of the "imposed" adverse pressure gradient and the wall induced pressure [f(x)].

However, the calculation results, shown in Figures 11 to 14, do allow examination of a key element of the problem--the modulation of the profile due to a spatial pressure oscillation during retardation.

When a compliant wall provides a drag reduction, it may do so in the same manner as in the "Toms' effect," by altering the turbulent production and decreasing the number of bursts (see Donohue, et al., 1972). Therefore, to alter the "turbulent events," the wave length of the wall motion should probably be the order of the retardation length, or less ($\Delta x^+_{maximum} \simeq 200 \rightarrow 500$). Also, if the major influence of the wall motion is in altering or modulating the imposed adverse pressure gradient, then the amplitude of the motion should be sufficient so that, with the wave length noted above, the $|dP/dx|$ generated by the wall motion is the order of the "imposed" adverse dP/dx. There are no similar order of magnitude inferences as to wave speed which are obvious to the present authors.

All the results shown in Figures 11 to 14 are for the $\overline{u'v'}/\overline{u'v}_{rms} = .05$ case. Figure 11 is a "no modulation" case (same as .05 case in Fig. 9, but more detailed) for comparison with the compliant wall cases shown in Figures 12 to 14. The first compliant wall case (which employs cosine wave modulation), Figure 12, has a wavelength of $\Delta x^+ = \lambda^+ = 440$ and an amplitude of $y^+ = 1.46$, giving a maximum dP/dx due to modulation (for this case of $\lambda^+ = 440$) which is twice the "imposed" adverse dP/dx. For the other cases (Figs. 13 and 14) the wavelengths of the cosine modulation on the pressure field were $\Delta x^+ = 220$ and 110, respectively. In these cases the amplitude of the wave was reduced so that the same modulation in pressure amplitude was obtained in each case, but with the smaller wavelength the derivatives were factors of two and four, respectively, times the $\lambda^+ = 440$ modulation case.

The influence of the simulated compliant wall induced pressure modulation upon the profile development during retardation is clearly apparent on Figures 12 to 14. The most spectacular effects occur for the small wavelength, highest $|dP/dx|$ case (Fig. 14). As expected, for large enough wall-motion-induced pressure modulation the profiles actually alternate between being more inflected and considerably less so, when compared to the orderly, unmodulated profile development shown in Figure 11.

The basic question to be answered is what influence could this profile modulation (caused by the simulated compliant wall pressure field) have upon the "tendency to burst"? Referring to Figure 7, if the burst formation could be delayed somewhat (until the favorable dP/dx occurs) some of the bursts or ejections might not occur at all, resulting in a reduction of $\overline{u'v'}_{rms}$ and C_f. From a quasi-steady stability theory point of view the profile modulation due to a compliant wall is destabilizing because lower minimum critical Reynolds numbers are produced in the adverse gradient portion of the modulation cycle. Using Lin's (1953) approximation for the minimum critical Reynolds number, the influence of the wavy wall can be calculated from the local velocity profiles and is shown in Figure 15.

However, a completely different indication is obtained from consideration of stability theory for unsteady flows, i.e., where the "mean profile" is modulated. For this case both theory (Von Kerczek and Davis, 1974; and Grosch and Salwen, 1968) and experimental evidence (Borisov and Rosenfel'd, 1971; Obremki and Fejer, 1967; and Sergeev, 1966) indicate that small perturbations or oscillations can actually increase the flow instability (see also the excellent review on this subject by Loehrke, Morkovin, and Fejer, 1970). Simplistically, the favorable gradient portion of the modulation could "interrupt" the disturbance amplification and thus delay the instability growth process. The trick evidently is to have a small amplitude oscillation. During large amplitude oscillations the adverse gradient or destabilizing portion of the cycle could become sufficiently unstable to allow a burst to occur before the favorable portion of the cycle could intervene.

The possible compliant wall stability theory approach just described differs from the classic work in this area (e.g., Burton, 1969; Linebarger, 1961; Karplus, 1966; Landahl, 1961; Kaplan, 1964) in three important aspects:

(1) The concept is applied to burst generation in the very near wall region of a turbulent boundary layer where only a small delay in amplification may be sufficient to cause a large change in Reynolds stress.

(2) The compliant wall motion assumed is of the resonant type, where a certain dominant wavelength, wave speed, and amplitude occur. This motion is not, as in the previous work, directly related to the local instantaneous disturbance field. That is, the present approach does not necessarily demand very low damping, fully compliant or flow triggered surfaces (assumed in most of the previous work).

(3) The profiles are allowed to change as $f(x,t)$. Indeed, this aspect may be the key to the entire mechanism.

This discussion of a "Possible Compliant Wall Turbulent Drag Reduction Mechanism" is completely tentative in nature. However, as will be shown in the next section of the paper, this mechanism is not inconsistent with the available compliant wall drag reduction cases and is probably worth further, more detailed study, including both nonlinear, unsteady flow stability theory calculations, and experiments designed around the order of magnitude wall motion necessary to alter the instability portion of the retardation/burst cycle, i.e., $\lambda^+ \simeq 20 \rightarrow 200$ and $h^+ \simeq .2 \rightarrow 2$.

Indications of the necessary surface wave speed could probably be obtained from unsteady stability theory, but a compromise will probably be necessary between the conflicting requirements of a fairly large wave speed ($C/u_\infty \simeq .4 \rightarrow .8$) to follow the "turbulent event" in space and time and the diminution in pressure modulation amplitude caused by increased wave speed.

5. EXPERIMENTAL RESULTS

Re-examination of Previous Successful Experiments

The question of whether or not surface motions could be excited which had short wavelength components of the type required by the tentative theory just presented is crucial in determining whether or not the proposed mechanism merits additional study. No positive answer can be given at this time, but there is some evidence which suggests such small λ motions could have occurred. The influence of a small air gap has already been discussed, and although wavelength control has not been established, frequency shifting was apparent. Even though the small air gap may be important in Blick's (1969) previous experiments, it cannot explain some of his earlier data. In this earlier work, Blick, et al. (1968) reported successful drag reduction experiments using membranes over relatively deep cavities with no elastic slab backing. Re-examination of those experiments therefore appears to be in order.

Blick's (1968) earlier experiments utilized a 0.638 by 0.181 m polyvinyl chloride membrane 0.064 mm thick in a wind tunnel with a free stream velocity of 11.6 m/sec. The boundary layer thickness at the center of the test surface was 2.5 cm and the rigid wall skin friction coefficient was 0.0037. Using these data, the wall length scale was 0.03 mm. Consequently, an x^+ of 100 corresponded to a length of 3 mm--a very short wavelength. If a hydrodynamic coincidence instability occurred rather than the more common static divergence, the desired wavelengths may have been set up.

Ordinarily, at wind tunnel speeds of 11.6 m/sec ($M_\infty \simeq 0$), the most common panel instability is static divergence. It is possible to design a structure which does not diverge statically in the flow speed range of interest. Since the polyvinyl chloride membrane is highly viscoelastic, its own internal damping may be capable of preventing the first mode static divergence instability, and another instability may have occurred. One possibility is hydrodynamic coincidence which occurs when the wave pattern has a wave speed which matches the free stream velocity. Blick's (1968) data has been examined to determine what wavelengths have apparent wave velocities matching the free stream.

Maximum drag reduction occurred in Blick's (1968) unbacked air cavity experiments when $T_x = 70$ N/m and $T_z = 15$ N/m. Assuming the wave speed is simply λf and $\lambda = L/n$, equation (1) can be solved for the case when $\lambda = 3$ mm and $\lambda f = 11.6$ m/sec. Then $f = 3870$ Hz and assuming $m = 1$, $\rho_s = 1250$ kg/m^3, Equation (1) yields $n = 166$, or $\lambda = 3.8$ mm. Conversely, setting $\lambda = 3$ mm, and $n = 213$, Equation (1) yields $f = 4960$ Hz. Since damping will lower the actual vibration frequency below the calculated value, these calculations tend to indicate hydrodynamic coincidence instabilities might be capable of producing the wave pattern required from the theory.

Whether an instability produced by wave speed matching the free stream velocity was actually pro-

duced is uncertain. Furthermore, the question of how a wave motion of that type could be excited must also be answered. The Strouhal number (based on boundary layer thickness) which characterizes a surface frequency of 3870 Hz is $2\pi f\delta/U_\infty = 53.3$ which is about forty times higher than the nominal peak in the turbulent wall pressure spectrum. Also, the influence of damping and bending stiffness (the polyvinyl chloride skin may act like a plate rather than a membrane at such short wavelengths) on the free stream matching wave speed has not been taken into account.

An air gap may have existed during the experiments reported by Fischer, et al. (1975) which showed a 60 percent reduction in Reynolds stress. In that work, they reported that experiments with a mylar skin attached to a polyvinyl chloride plastisol substrate (which was naturally sticky) were strongly influenced by temperature. In fact, large Reynolds stress reductions seemed to occur only when the wind tunnel had been cooled to temperatures below 10°C (which occurred in February). The thermal coefficient of expansion of polyvinyl chloride plastisol is such that a 10°C reduction in temperature could have shrunk the substrate sufficiently to pull it away from the mylar skin. If such a separation occurred, the mylar skin would have been over a small air gap until the tunnel warmed sufficiently for it to reattach. The last series of tests were conducted in June, no cold tunnel conditions occurred, and no large Reynolds stress reductions were measured.

The active wall experiments of Mattout (1972) also can be interpreted as a short wavelength phenomenon. In his experiments with fully turbulent water boundary layers, he found that mechanically produced waves could actually produce a thrust. His waves were produced by mechanically driven rods attached to a 1-meter-long mylar skin. The rods were 7 mm apart and a large thrust (five times greater than the original drag) was produced when waves with frequencies of 23 Hz and a wave speed of 12.2 m/sec (in either direction) were driven beneath a turbulent boundary layer (Reynolds number based on length was 2.4×10^6 at the beginning of the active wall and 4×10^6 at the trailing edge). The wavelength was 0.525 m and the amplitude was 1 mm. The free stream velocity was 1.58 m/sec and the average boundary layer thickness was 3.7 cm. Using a calculated rigid wall skin friction coefficient of 0.0031, the wall length scale for these experiments was 0.016 mm.

If the very long wavelength reported by Mattout (1972) is replaced by the distance between rods, the wavelength is 7 mm. A 7 mm wavelength corresponds to a λ^+ of about 430 which is in the theoretically suggested range of interaction. Furthermore, the wave speed of $0.1\ U_\infty$ based on the rod spacing wavelength is in line with the theoretically suggested value.

Certainly the flow resonance phenomena produced by a mechanically driven wall is different than the coupled fluid-solid resonance required for a compliant wall. However, the inter-rod interaction calculations suggest that controlled short wavelength surface motions, of the type suggested by the theory, are capable of profoundly altering the structure of a turbulent boundary layer. The question is, were inter-rod motions responsible for the favorable interaction?

At this point, it is obvious that many serious questions exist concerning the present tentative mechanism of compliant wall drag reduction. (Although probably no more serious than any previously suggested model.) The only way these questions will be answered is by detailed simultaneous measurements of the turbulent flow and wall motions. High resolution wall measurements will be required if the wavelengths suggested by the theory are important. Those measurements must be taken during a known successful drag reduction experiment and conditional sampling will probably be required. The problem then is simultaneous measurement of (1) a large drag reduction, (2) accurate instantaneous fluid velocities at locations affected by the monitored wall motion, (3) spatial and temporal variations of the surface, and (4) accurately determined mechanical properties of the successful surface and temporal variations of the surface motion. The section which follows represents an initial attempt at simultaneous measurements of several aspects of the problem.

Present Experiments

The experiments reported here represent a continuation of the low-speed program reported by Fischer, et al. (1975). However, a more detailed and direct approach was utilized in the experimental measurements. The models and test conditions are briefly summarized in Tables 2 and 3 respectively. In addition to the Reynolds stress and pitot measurements previously employed, the present study has included some surface motion measurements and measurements of membrane tension.

A different approach was used to analyze the data which permitted rapid determination of any significant reductions in Reynolds stress. Rather than employ large numbers of detailed boundary layer surveys to determine when drag reduction occurred, the swept hot-

wire and pitot probes were positioned at a fixed height of 0.4 cm above the surface and wind tunnel speed was varied. A computer with an x-y plotter was connected directly to the instrument outputs and an approximate equation to compute Reynolds stress was employed to produce an on-line record of near wall Reynolds stress as a function of free stream velocity. By comparing the compliant wall plots with the previously generated rigid wall data, an immediate indication of changes in Reynolds stress could be determined. If a significant decrease or increase in Reynolds stress occurred, detailed boundary layer and surface measurements were taken.

Unfortunately, no large decreases in Reynolds stress were measured during this entry and the experiments generally utilized preselected velocities for detailed survey measurements. About 20 data points were taken in each boundary layer survey with measurements as close as 0.2 cm from the wall. Details of the hot-wire Reynolds stress probe, pitot probe, and survey mechanism are given in Fischer, et al. (1975).

New Instrumentation: Because the mylar skin was so thin, conventional strain gages could not be used to determine skin tension. Fine wires about 10 cm in length were therefore cemented directly to the back of the mylar skin and used as strain gages. Two wires were used on each surface to measure longitudinal and lateral tension. The mylar skin was hand stretched and taped to the model frame, resulting in some control over the tension. For some of the models, the mylar was stretched several times in order to vary the tension.

Surface motion was measured using the detection system shown schematically in Figure 16. Actually, dual light sources and cutoffs were used. One of the light sources was continuous and was used with a photodetector to monitor continuously the surface motion of a 0.5 cm diameter spot on the compliant surface. The other light source was a Xenon flash lamp with a 1-μsec duration which was used with a camera to record the instantaneous surface pattern over a 15 by 20 cm area of the model. The cutoffs were radial graded filters, with transmission varying linearly from a maximum at the centerline to zero at the outer edge. That filter produced linear results for local surface deflection angles between ± 0.3°. The principle of operation was essentially the same as a Schlieren system but over a far greater dynamic range.

Reynolds Stress Data Reduction: Since the hot-wire data were linearized (although not perfectly), for the purposes of preliminary data analysis, an exact linearization was assumed. Using that assumption, the dimensionless Reynolds stress equation in Fischer, et al. (1975) can be approximated by

$$\frac{-2\overline{u'v'}}{U_\infty^2} \simeq \left(\frac{u_\ell}{U_\infty}\right)^2 \frac{e_+^2 - e_-^2}{\overline{V}_{av}} \tag{9}$$

where the local velocity (u_ℓ) and tunnel velocity (U_∞) were obtained from pitot data. Equation (9) was used in the on-line Reynolds stress calculations mentioned previously.

Final Reynolds stress reduction was accomplished by allowing for nonlinearity in the hot-wire calibration. Then, the appropriate relationship was

$$\frac{-2\overline{u'v'}}{U_\infty^2} = \left(\frac{du_\ell}{d\overline{V}_{av}}\right)^2 \frac{e_+^2 - e_-^2}{U_\infty^2} \tag{10}$$

where local velocity (u_ℓ) was determined from the hot wire.

Equation (10) is still not exact because the swept hot wire was not infinitely long, perfectly straight, or inclined at exactly 45° to the flow. However, those corrections would produce a correction constant near unity for each individual hot wire. Hence, comparison between the rigid plate and compliant surface could be made with a high degree of accuracy for a single hot wire.

Results and Discussion

As mentioned previously, no large Reynolds stress reductions were recorded and consequently, the surface motion measurements were made at representative test conditions rather than during drag reduction. Measurements at this stage are qualitative and are used here only for discussion. Furthermore, the optical system utilized during the experiments was designed for large wavelength motion analysis and was only capable of resolving wavelengths between 2 and 20 cm, which precludes detection of short wavelength motion suggested by the mechanism discussed herein.

Figure 17 shows instantaneous surface angle distributions for four of the surfaces. The surface shown in Figure 17a gives an indication of the surface tension induced curing pattern on the bare polyvinyl chloride plastisol (PVC Plastisol) rather than wave motion. The motion induced pattern was not directly visible and thus the flaws effectively prevented surface measurements. Some surface deflection is apparent in Figure 17b, but much of the pattern is a result of the porous substrate rather than surface motion. Only

slight motion is obvious for low speed flow over the membrane strip shown in Figure 17c, but a large wavelength pattern of large amplitude is obvious at the higher velocity shown in Figure 17d. The threefold increase in dynamic pressure shows a pronounced effect.

Continuous measurements of surface angle over a 0.5-cm-diameter circle were capable of giving usable results in most cases, even when area pictures were unsatisfactory. Time histories of the type shown in Figure 18 could then be generated. From the time scale, frequencies from 20 to about 1000 Hz can be resolved. The amplitude of the motion on the full size membrane varied significantly with velocity but power spectra indicated a narrow frequency response interval which varied between 40 and 80 Hz, depending on U_∞. Higher frequencies seem to be superimposed on the original low frequency motion for the membrane strip shown in Figure 18b as velocity was increased. However, the presence of the large amplitude low frequency motion does not appear to allow a favorable compliant effect for either of the membrane cases. Frequencies in the interval between 300 and 600 Hz are indicated on the PVC plastisol with membrane and the laminated surface. However, amplitudes were so small that only slight interaction may have taken place. Furthermore, because of the size of the sensing spot, higher frequency low wavelength motions could have escaped detection.

The results of the surface motion photographs and photodetector allowed the surface wavelengths and maximum amplitudes to be determined in some cases. For example, if the area photo and photodetector indicated excursions through the maximum sensing angles, wavelengths could be measured from the photograph and the maximum amplitude is approximately found from

$$a_{max} \approx \frac{\lambda}{3} \tan \theta_{max} \quad .$$

When the wavelength could not be determined from the photograph the wave speed had to be estimated to determine λ and a_{max}. The result of the surface motion is shown in Table 4. Wave speeds of $\approx .5\ U_\infty$ were used when not known, and this may be considerably in error.

The tension was adjusted for several models and a range of from 17.5 to about 350 N/m was covered. Later, models were run without strain gages because the wires seemed to alter surface motion, and tension was estimated for these cases. Since these latter models showed small drag reduction, the applied tension could only be characterized as low or high, where low is generally loadings below 50 N/m, and high is above that level.

Although the tension did not affect the theoretical values of the vibration modes to a large degree, the amplitude of the surface motion appears to vary. At this time the data is too badly scattered to draw strong conclusions on the influence of tension except to note that a slight drag reduction occurred for low tension on the laminated foam structure and the PVC with membrane, while no drag reduction occurred for the higher tension.

The only drag reduction which occurred was for the low tension Scottfelt and PVC with membrane tests which are shown in Figure 19. Here the assumption is made that the ratio of Reynolds stresses at a fixed small distance from the wall is equal to the ratio of wall shear stress (ratio to rigid reference plate). The surveys (here and in Fischer, et al., 1975) showed that the value of $-2\overline{u'v'}/U_\infty^2$ was nearly constant near the wall. Thus the plot of Figure 19 gives τ_w/τ_{wFP} against U_∞ for the two models mentioned. The expected accuracy of this data is ± 4 percent, so the drag reduction indicated is only marginally detectable within the accuracy of the instrumentation. It should be pointed out that the Scottfelt model data does tend to agree with the same case in Fischer, et al. (1975), and thus may be more conclusive. The failure of the PVC model with the membrane to give the large reductions previously reported may be due to the greatly different temperatures, or other unknown factors (such as possible delamination).

6. DISCUSSION AND CONCLUSIONS

The purpose of this work has been to give a somewhat detailed status report of the effort at Langley Research Center to identify and isolate the compliant wall drag reduction phenomenon. Compliant wall-fluid interactions have been extremely difficult to study because of a complete lack of surface motion data during successful experiments and, as a result, no definite clues on the specific mechanism are available. The techniques reported here allow the compliant wall problem to be approached from three directions--numerical simulation of structural motions, fluid-structure modeling, and simultaneous experimental measurement of fluid velocity and surface motion.

The NASTRAN finite element program has been found capable of handling composite structural design concepts in both natural frequency calculations and transient simulations. The resulting transient calculations can be used in either turbulent pressure simulations (uncoupled or coupled) or in spectral analysis for comparison with experimental data.

A new conceptual compliant surface drag reduction mechanism based on the stability of the turbulent substructure has been proposed and an analysis of previous successful experiments was employed to identify specific wavelength ranges for desired surface motion. These guidelines have been used to identify specific design criteria and various compliant wall structural design concepts have been evaluated.

Three types of potential compliant surface designs have been identified. The backed membrane which is not attached to its elastic substrate (membrane with air gap) appears to allow both wavelength and frequency control and is supported by the largest amount of successful experimental data. The laminated structural concept is more desirable as a realistic surface, but experimental configurations employed thus far indicate less motion control (based on eigenvalue calculations). Some experimental data exists which indicates modest reductions in skin friction over laminated surfaces, but the high substrate damping appears to retard effective amplification of desired wall motions. The periodic structure is a newly identified design concept which appears to combine durability with wavelength and frequency control and will be tested in the near future.

An experimental approach has been employed to identify significant reductions in Reynolds stress while the test is in progress--thereby permitting detailed studies of the interaction when it occurs. Unfortunately, the drag reductions which occurred during these tests were so small that they were only detected in final, detailed Reynolds stress data reduction. Temporal and spatial variations in surface elevation have been measured optically and a higher resolution version of the technique should supply the data required for isolating the compliant wall phenomenon.

SYMBOLS

a	amplitude
c	wave speed
c_f	skin friction coefficient
c_p	pressure coefficient
D	plate stiffness
E	Young's modulus of elasticity
$\overline{e_+^2}$	average squared hot-wire voltage fluctuation at +45° to mean flow
$\overline{e_-^2}$	average squared hot-wire voltage fluctuation at -45° to mean flow
f	frequency or eigenvalue
H	slab thickness
h	skin thickness
h^+	dimensionless wave height
L	length of compliant surface
M	Mach number
m,n	wave numbers
P	pressure
T	tension
t	time
U_∞	free stream velocity
u'	velocity fluctuation in x-direction
u_τ	friction velocity
$\overline{V}_{av}$	average hot-wire voltage
v'	velocity fluctuation in y-direction
W	width of compliant surface
x	coordinate in direction of flow
x^+	xu_τ/ν
y	coordinate perpendicular to surface
y^+	yu_τ/ν
z	transverse coordinate
β	damping coefficient
Γ	reciprocal wave number
γ.	gap thickness
δ	boundary layer thickness
ζ	vertical surface displacement
λ	wave length
λ^+	dimensionless wave length
ν	kinematic viscosity
ν_s	Poisson's ratio for the skin
ρ	density
σ	$\sqrt{1 - M_\infty^2}$
ω	radian frequency

Subscripts

conv.	convection
e	boundary layer outer edge
f	foam or substrate
ℓ	local

o reference

rms root mean square

s skin

w wall

∞ free stream

REFERENCES

Ash, R.L., 1974, "On the Theory of Compliant Wall Drag Reduction in Turbulent Boundary Layers", NASA Contractor Rep., No. CR-2387.

Babenko, V.V., 1973, "Technique for Determining the Mechanical Properties of Flexible Coatings and a Basis for Their Selection and Design" (In Russian) Bionika, 7, 71.

Blackwelder, R.F., and Kaplan, R.E., 1971, "Intermittent Structures in Turbulent Boundary Layers", AGARD Conf. Paper, no. CP-93.

Blick, E.F., Vert, C.W., Reed, T.D., Walters, R.R., and Wares, R.N., 1968, "Aerodynamic Drag Reduction Using Compliant Coatings", Proc. Okla. Acad. Sci., 47, 429.

Blick, E.F., Walters, R.R., Smith, R., and Chu, H.H., 1969, "Compliant Coating Skin Friction Experiments", A.I.A.A. Paper, no. 69-165.

Borisov, Vu.Ya., and Rosenfel'd, E.I., 1971, "Action of Acoustic Oscillations on Flow Stability and Structure", Soviet Physics-Acoustics, 17, 154.

Burden, H.W., 1969, "The Effect of Wall Porosity on the Stability of Parallel Flows Over Compliant Boundaries", Ph.D. Thesis, University of Pennsylvania.

Burton, T.E., 1974, "The Connection Between Intermittent Turbulent Activity Near the Wall of a Turbulent Boundary Layer with Pressure Fluctuations at the Wall", M.I.T. Tech. Rep., no. 70208-10.

Bushnell, D.M., and Beckwith, I.E., 1970, "Calculation of Nonequilibrium Hypersonic Turbulent Boundary Layers and Comparison with Experimental Data", A.I.A.A.J., 8, 1462.

Corino, E.R., and Brodkey, R.S., 1969, "A Visual Investigation of the Wall Region in Turbulent Flow", J. Fluid Mech., 30, 741.

Donohue, G.L., Tiederman, W.G., and Reischman, M.M., 1972, "Flow Visualization of the Near Wall Region in a Drag Reducing Channel Flow", J. Fluid Mech., 56, 559.

Dowell, E.H., 1970, "Panel Flutter: A Review of the Aeroelastic Stability of Plates and Shells", A.I.A.A.J., 8, 385.

Ffowcs-Williams, J.E., 1964, "Reynolds Stress Near a Flexible Surface Responding to an Unsteady Flow", Bolt, Beranek and Newman, Inc. Rep. no. 1138.

Fischer, M.C., Weinstein, L.M., Ash, R.L., and Bushnell, D.M., 1975, "Compliant Wall Turbulent Skin Friction Reduction Research", A.I.A.A. Paper, no. 75-833.

Grass, A.J., 1971, "Flow Over Smooth and Rough Walls", J. Fluid Mech., 50, 233.

Grosch, C.E., and Salwen, H., 1968, "The Stability of Steady and Time Dependent Plane Poiseuille Flow", J. Fluid Mech., 34, 177.

Hansen, R.J., and Hunston, D.L., 1974, "An Experimental Study of Turbulent Flow Over Compliant Surfaces", J. Sound Vib., 34, 297.

Inger, G.R., and Williams, E.P., 1972, "Subsonic and Supersonic Boundary Layer Flow Past a Wavy Wall", A.I,A.A.J., 10, 636.

Kaplan, R.E., 1964, "The Stability of Laminar Incompressible Boundary Layers in the Presence of Compliant Boundaries", A.S.R.L. Tech. Rep., no. TR116-1.

Karplus, H.B., 1966, "Turbulent Flow Transition Near Solid anf Flexible Boundaries", I.I.T. Res. Inst. Proj. Rep., no. M-6110.

Kendall, J.M., 1970, "The Turbulent Boundary Layer Over a Wall with Progressive Surface Waves", J. Fluid Mech., 41, 259.

Kim, H.T., Kline, S.J., and Reynolds, W.C., 1971, "The Production of Turbulence Near a Smooth Wall in a Turbulent Boundary Layer", J. Fluid Mech., 50, 133.

Kline, S.J., Reynolds, W.C., Schraub, F.A., and Runstadler, P.W., 1967, "The Structure of Turbulent Boundary Layers", J. Fluid Mech., 30, 741.

Kobashi, Y., Hayakawa, M., and Nakagawa, K., 1975, "Development of Disturbances in Unsteady Boundary Layers", Proc. Symp. Unsteady Aerodynamics, sponsored by USAF-AFOSR and Univ. Arizona.

Kolsky, H., 1953, Stress Waves in Solids, Oxford Press.

Kramer, M.O., 1965, "Hydrodynamics of the Dolphin", in Advances in Hydrosciences, Vol. 2, p. 111, Academic Press.

Landahl, M.T., 1961, "On the Stability of a Laminar Incompressible Boundary Layer Over a Flexible Surface", J. Fluid Mech., 13, 609.

Leehey, P., and Davies, H.G., 1975, "The Direct and Reverberant Response of Strings and Membranes to Convecting Random Pressure Fields", J. Sound Vib., 38, 163.

Levchenko, V.Ya., and Solov'ev, A.S., 1972, "Boundary Layer Stability on a Wavy Periodic Surface", Fluid Dynamics, 7, 884.

Lin, C.C., 1955, The Theory of Hydrodynamic Stability, p. 83, Cambridge Univ. Press.

Linebarger, J.H., 1961, "On the Stability of a Laminar Boundary Layer Over a Flexible Surface in a Compressible Fluid", M.S. Thesis, M.I.T.

Loehrke, R.I., Morkovin, M.V., and Fejer, A.A., 1970, "New Insights on Transition in Oscillating Boundary Layers", A.F.O.S.R. Scientific Rep., no. AFOSR 70-1586 TR.

MacNeal, R.H., 1972, NASTRAN Theoretical Manual (Level 15.0), Sci. Tech. Inf. Office, N.A.S.A., Wash., D.C.

Mattout, R., and Cottenceau, B., 1972, "Etude experimentale d'une paroi souple activee en tunnel hydrodynamique mesures globale", Societé Bertin and Cie, Note technique, no. 71-C1-09.

McAlister, K.W., and Wynn, T.M., 1974, "Experimental Evaluation of Compliant Surfaces at Low Speeds", N.A.S.A. Tech. Memo., no. TMX-3119.

Newmark, N.M., 1959, "A Method of Computation for Structural Dynamics", J. Engg. Mech. Div. A.S.C.E., EM-3, 67.

Nonweiler, T., 1963, "Qualitative Solution of the Stability Equation for a Boundary Layer in Contact With Various Forms of a Flexible Surface", A.R.C. Rep., no. CP-622.

Obrenski, H.J., and Fejer, A.A., 1967, "Transition in Oscillating Boundary Layer Flows", J. Fluid Mech., 29, 93.

Offen, G.R., and Kline, S.J., 1973, "Experiments on the Velocity Characteristics of 'Bursts' and on the Interaction Between the Inner and Outer Regions of a Turbulent Boundary Layer Flow", Thermosciences Div. Mech. Engrg. Dept. Stanford Univ. Rep., no. MD-31.

Rogers, K.H., 1974, "Boundary Layer Theory for Pressure and Drag of a Wavy Surface", J. Aircraft, 11, 382.

Saxena, S.K., and Bose, T.K., 1974, "Numerical Study of the Effect of Pressure Gradient on Stability of an Incompressible Boundary Layer", Phys. Fluids, 17, 1910.

Sergeev, S.I., 1966, "Fluid Oscillations in Pipes at Moderate Reynolds Numbers", Fluid Dynamics, 1, 121.

Shapiro, H., 1954, The Dynamics and Thermodynamics of Compressible Fluid Flow, Vol. 1, p. 313, Ronald Press.

Shemdin, O.H., and Hsu, E.Y., 1967, "Direct Measurement of Aerodynamic Pressure Above a Simple Progressive Gravity Wave", J. Fluid Mech., 30, 403.

Von Kerczek, C., and Davis, S.H., 1974, "Linear Stability Theory of Oscillatory Stokes Flow", J. Fluid Mech., 62, 753.

Wallace, J.M., Eckelman, H., and Brodkey, R.S., 1972, "The Wall Region in a Turbulent Shear Flow", J. Fluid Mech., 54, 39.

Willmarth, W.W., and Lu, S.S., 1972, "Structure of the Reynolds Stress Near the Wall", J. Fluid Mech., 55, 65.

Yu, H.Y., and Hsu, E.Y., 1971, "A Refined Measurement of Aerodynamic Pressure Over Progressive Water Waves", Dept. Civil Engng, Stanford Univ. Tech. Rep., no. 16.

Yu, H.Y., Hsu, E.Y., and Street, R.L., 1973, "Wave Induced Perturbations in a Turbulent Boundary Layer Over Progressive Water Waves", Dept. Civil Engng., Stanford Univ. Tech. Rep., no. 172.

Table 1. Representative Eigenvalue Calculations

Eigenvalues Arranged in Ascending Order	Model and Method of Calculation				
	(a) Membrane	(b) Elastic Slab	(c) Laminated Structure		(d) Periodic Structure
	Eqn. (1)	Eqn. (2)	Eqn. (3)	NASTRAN	NASTRAN
f_1	85.85 Hz	1033	484.6	453.3	5686
f_2	97.89	2066	485.0	453.6	7473
f_3	115.18	3010	485.7	454.1	7475
f_4	135.75	4133	486.6	455.2	7477
f_5	158.31	5166	486.6	456.4	
f_6	165.14	6199	487.7	458.0	
f_7	171.71	7232	488.9	459.3	
f_8	182.12*	8265	490.4	459.5	
f_9	182.12*	9299	490.5	461.24	
f_{10}	195.78	10332	492.0	461.32	15621†

* Identical eigenvalues.

† Number of eigenvalues between 5686 and 15621 depends on number of ribs.

Table 2. Models Tested

Substrate of Compliant Wall	Surface Covering	Bonding Agent	Remarks
Rigid aluminum plate	None	None	Reference surface
0.64-cm-thick, 90 PPI compressed polyurethane foam (Scottfelt)	0.0025-cm-thick mylar membrane	0.050-cm-thick RTV silicone rubber	Old model with thinner RTV bond (showing some drag reduction) as well as new model were run. Tension was varied.
0.64-cm-thick polyvinyl chloride plastisol (PVC)	None	None	Surface had slight irregularities, but not enough to cause roughness effects to be large.
0.64-cm-thick polyvinyl chloride plastisol (PVC)	0.0025-cm-thick mylar membrane	PVC naturally adhesive	Membrane smoothed out irregularities even under low tension. Several tensions run.
0.64-cm-thick 100 PPI polyurethane foam	0.0025-cm-thick mylar membrane	None	Small air gap was desired, but under flow, surface bulged so as to make gap uncontrolled.
15.2 x 130 cm air back (strip membrane)	0.0025-cm-thick mylar membrane	---	Strip model had three longitudinal strips with membrane bonded to dividers.
45 x 130 cm air back (full membrane)	0.0025-cm-thick mylar membrane	---	Full area pure membrane.

Table 3. Flow Conditions.

x_{probe}	y_{probe}	m_∞	U_∞	$T_{t\infty}$	R_∞/m	P_∞
108 cm	0.2 to 6.25 cm	0.05 to .36	17 to 122 M/sec	300° to 315°K	0.094×10^6 to $.668 \times 10^6$	1 atm

Table 4. Surface Motion Results.

Model	(m/sec) U_∞	Measured Frequencies	≈Max. Amplitude	≈λ's
Mylar Membrane	31 49	40 Hz 80	0.017 cm 0.034	20 cm 20
Strip Mylar Membrane	31 55	38 40 (and some at 180)	0.012 0.040	30 ≤30
PVC with Membrane	31 61 91	several Bands up to 300 Hz	0.0002 0.0005 0.0007	≥3
Scottfelt	31 61 91	several Bands up to 600 Hz	0.0002 0.0005 0.0007	≥1.5

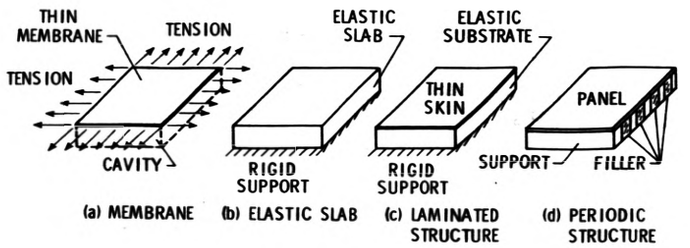

Figure 1. Basic Compliant Wall Design Concepts

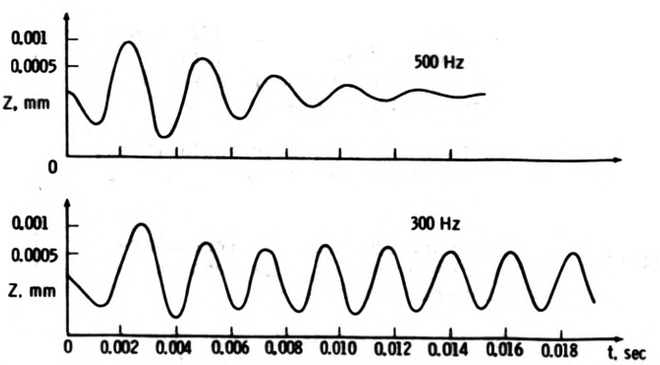

Figure 2. Local Surface Motion Resulting from a Convected Pressure Fluctuation

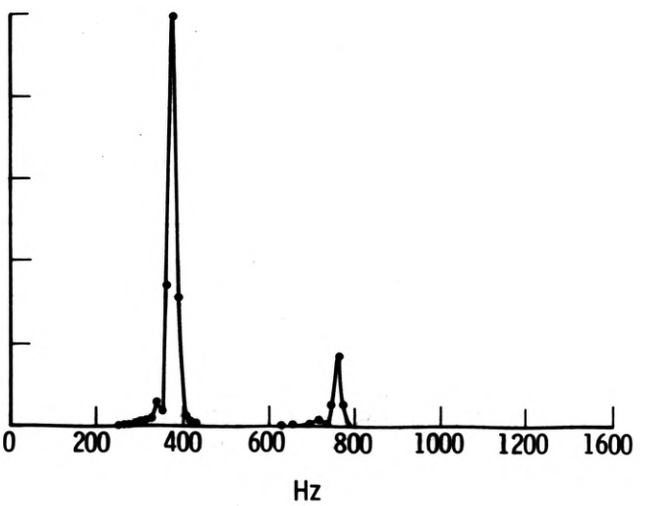

Figure 3. Surface Motion Spectrum for a 300 Hz Convected Pressure Fluctuation

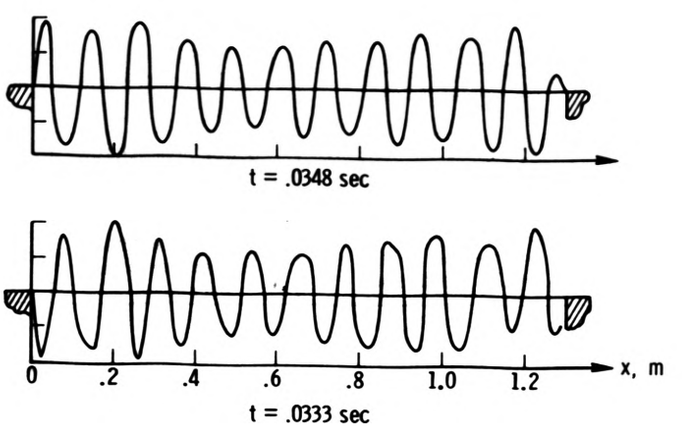

Figure 4. Instantaneous Surface Configuring at Consecutive Time Steps

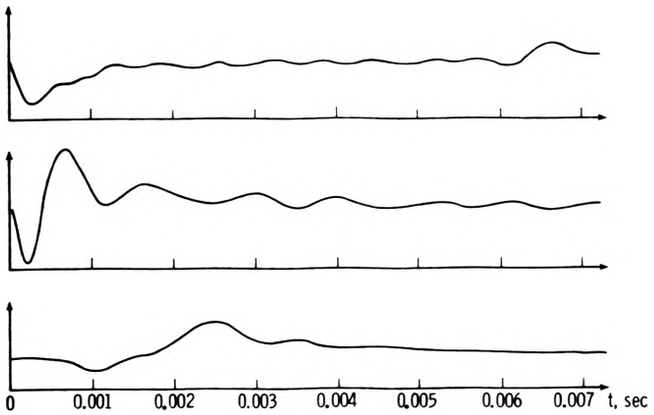

Figure 5. Centerline Surface Motion on a Membrane (a) Solution from Equation (6), (b) Impulsive Load, Small Air Gap, (c) Convected Pressure Fluctuation

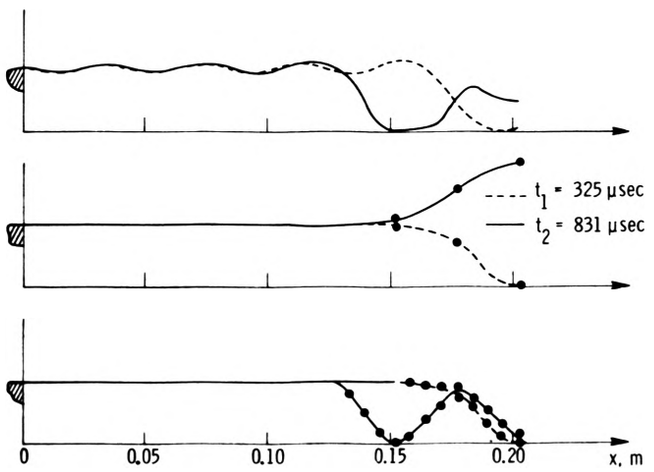

Figure 6. Influence of Node Spacing on Membrane Surface Patterns (a) Solution from Equation (6), (b) Numerical Solution: 2.5 x 2.5 cm Network, (c) Numerical Solution .63 x .63 cm Network

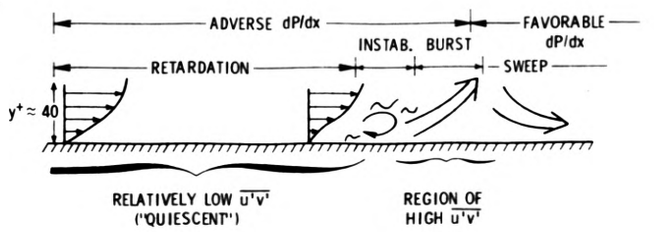

Figure 7. Sketch of Possible Turbulent Event Cycle from Kline, et al. (1967), Burton (1974)

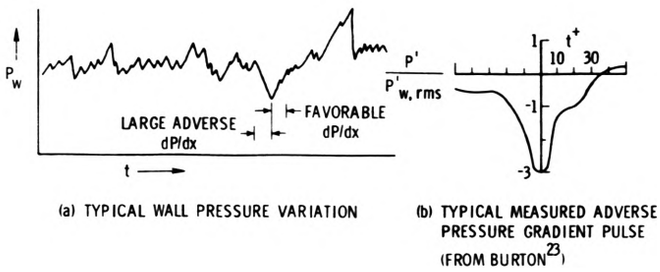

Figure 8. Pressure Variation Imposed on Wall Region by Large Scale Motions in the Outer Flow ($y^+ \cong 400$)

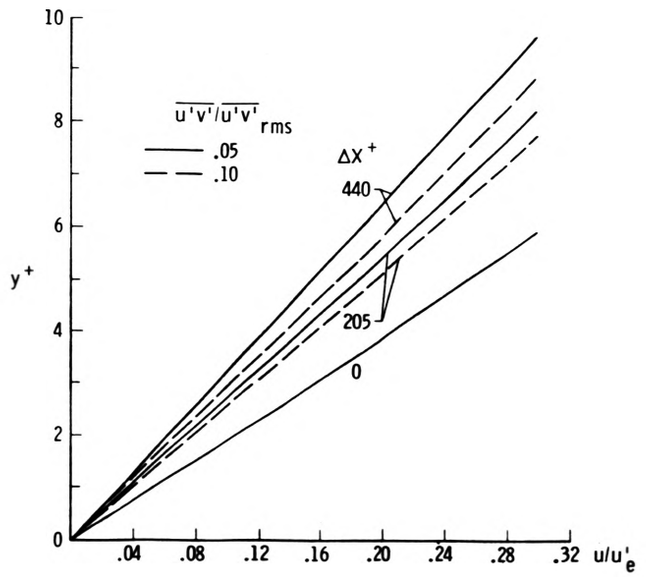

Figure 9. Quasi-Steady Retardation Calculations, Using dP/dx from Burton (1974), Smooth Wall

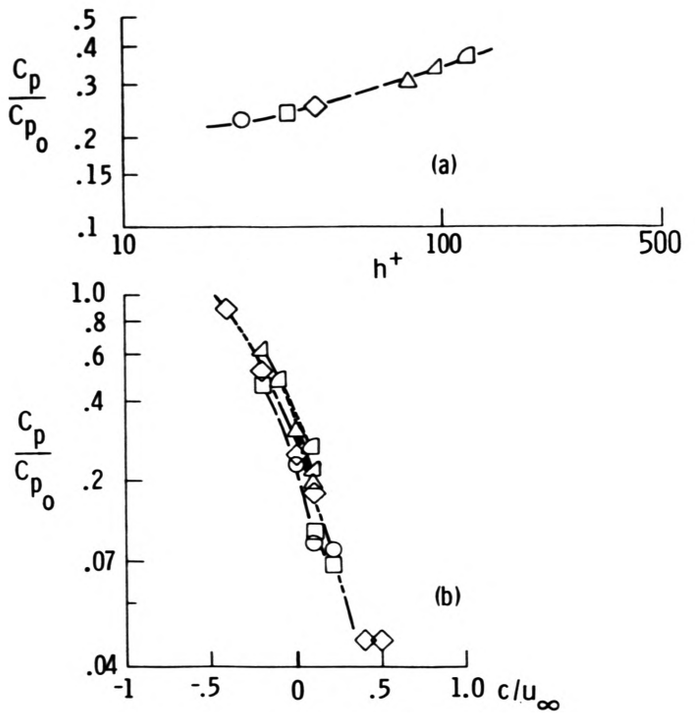

Figure 10. Influence of Wave Speed and Non-Dimensional Wave Height Upon Normalized Peak Pressure Over a Wavy Wall, From Kendall (1970)

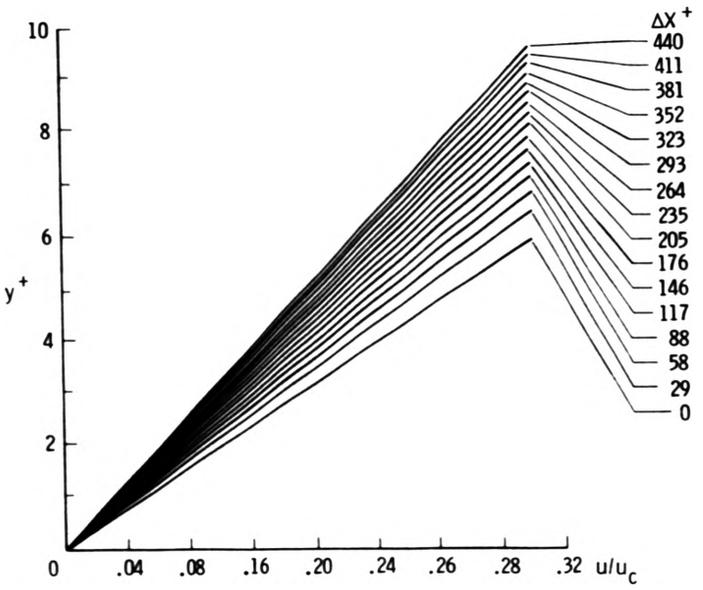

Figure 11. Quasi-Steady Retardation Calculations, Smooth Wall, $\overline{u'v'}/\overline{u'v'}_{rms}$ = .05

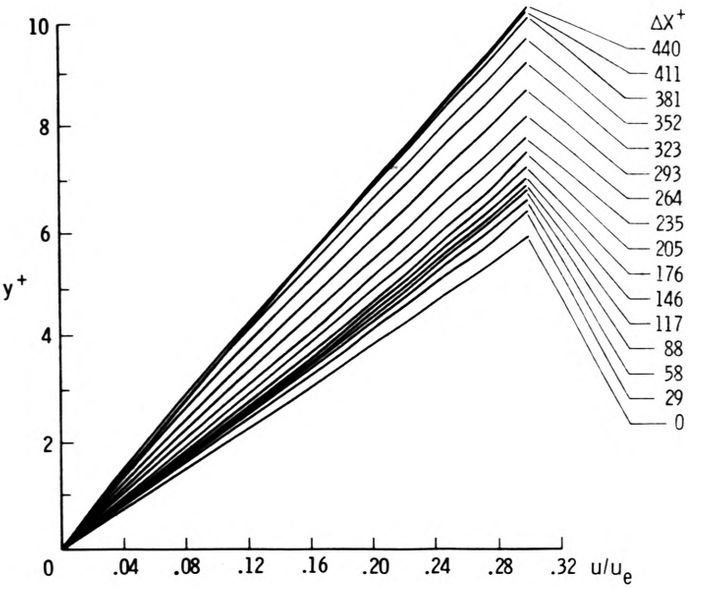

Figure 12. Quasi-Steady Retardation Calculations, $\overline{u'v'}/\overline{u'v'}_{rms}$ = .05, λ^+ = 440

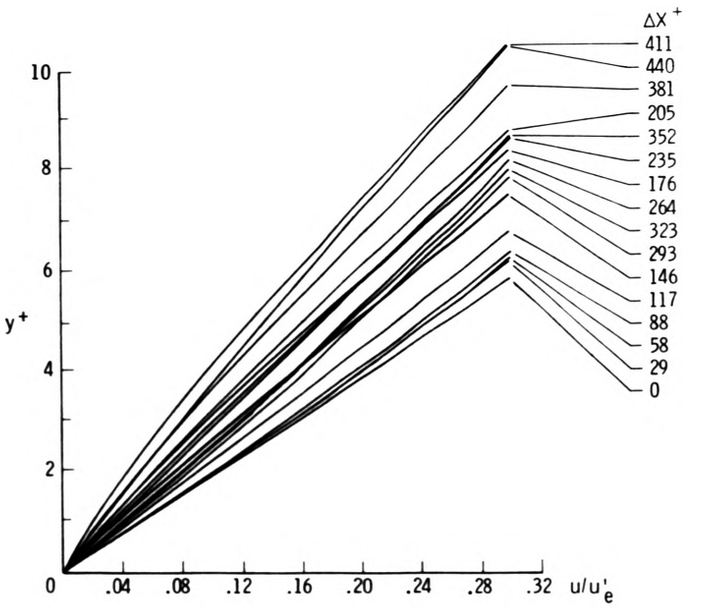

Figure 13. Quasi-Steady Retardation Calculations, $\overline{u'v'}/\overline{u'v'}_{rms}$ = .05, λ^+ = 220

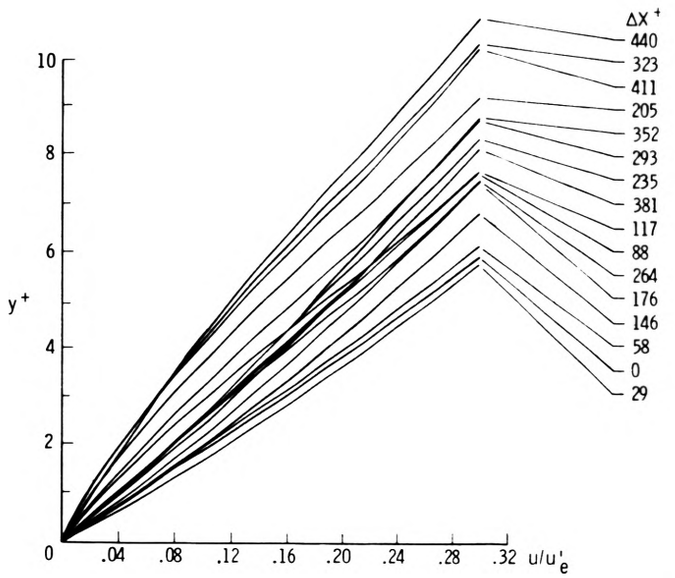

Figure 14. Quasi-Steady Retardation Calculations, $u'v'/u'v'_{rms} = .05$, $\lambda^+ = 110$

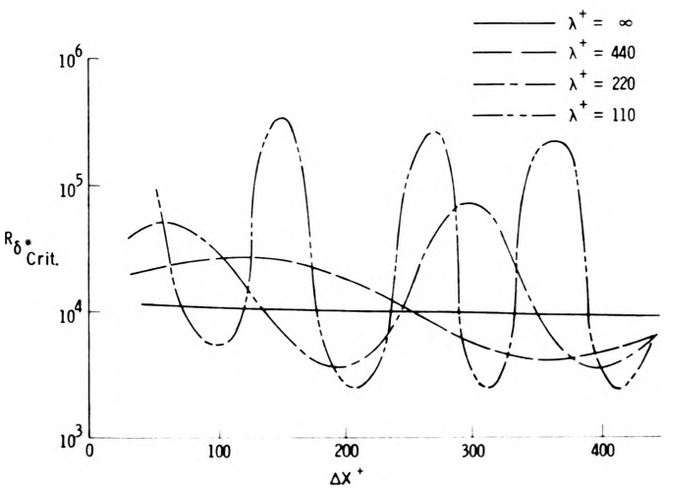

Figure 15. Influence of Pressure Modulation on Local Minimum Critical Reynolds Number

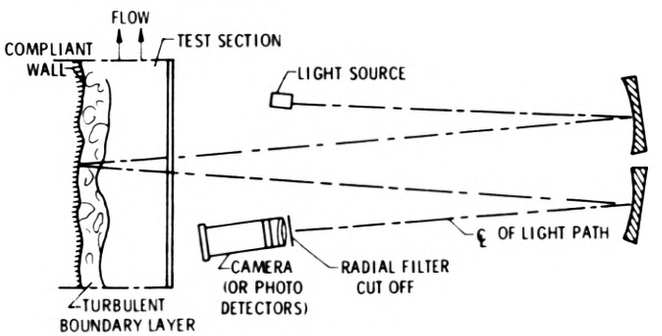

Figure 16. Compliant Wall Schlieren Surface Motion Apparatus (Top View)

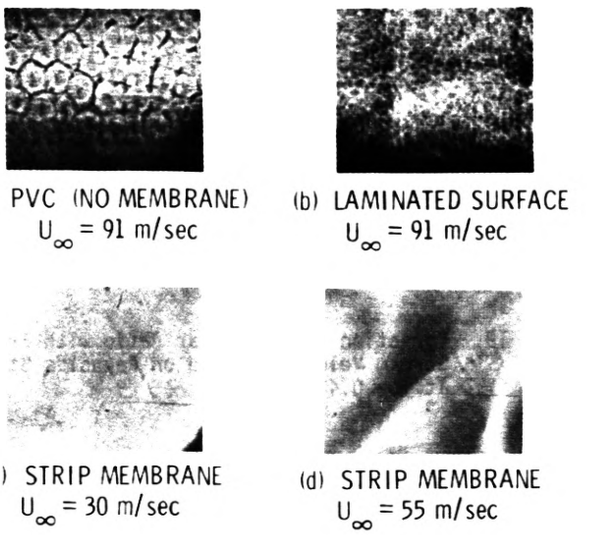

Figure 17. Photographs of Surface Motion Pattern for Several Models: Exposure Time 1 μsec, Area Shown 12 x 15 cm

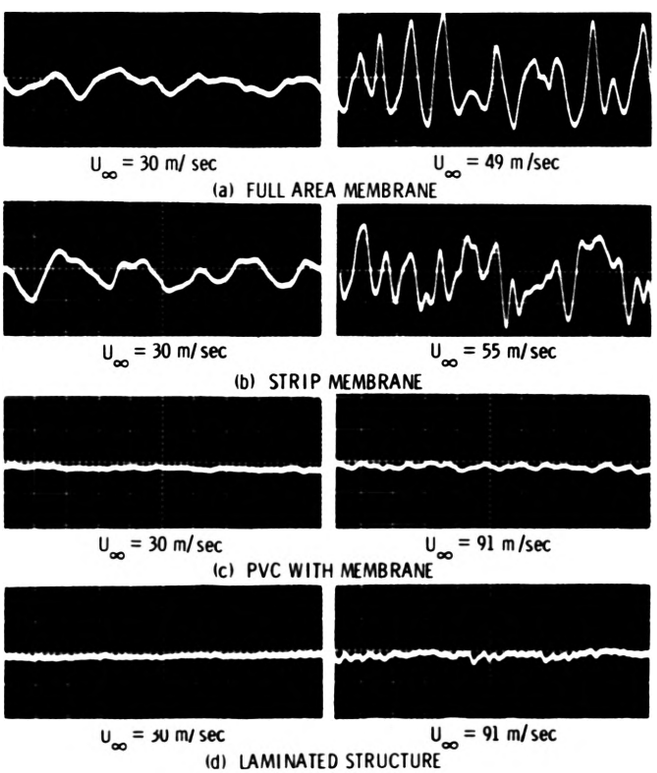

Figure 18. Surface Inclination History of 0.5 cm Spot on Several Models. Full Scale Corresponds to ± 0.3° Deflection

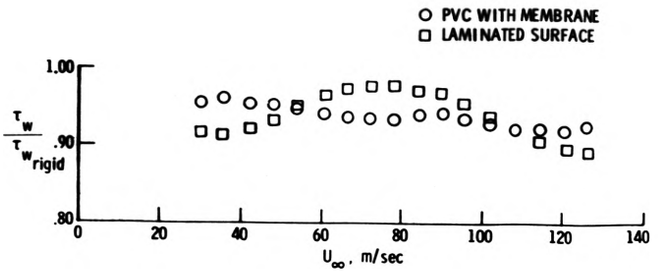

Figure 19. Variation of Wall Shear Ratio with Free Stream Velocity; Based on Reynolds Stress at y = 0.4 cm

DISCUSSION

H. M. Fitzpatrick, ONR: Could you explain further the distinction between "resonant" and "triggered" passive responses of a compliant membrane?

Ash: The original idea of a compliant surface was a surface which when exposed to a sudden pressure fluctuation responded locally to that pressure fluctuation. That surface is at least theoretically possible to produce in water where you have very large dynamic pressures. But the pressure fluctuations in air are of such low magnitude (the Q is so small) that we don't believe it is possible to get enough force on a surface to cause it to deform locally even with a small Y^+. We could get a large Y^+ if we had true panel flutter. We believe what in fact gets set up is a form of panel flutter. That is the surface is not responding locally to an instantaneous pressure fluctuation but is excited resonantly due to a particular band of frequencies in the turbulent boundary layer and operates on an essentially continuous basis. There is some continuous surface motion that is set up on a global sense and not on a local sense.

W. Willmarth, Univ. of Michigan: Could you speculate about the mechanisms of those methods responsible for C_f reduction when the compliant surface is effective? I am referring to the configurations on the next to the last slide.

Ash: I think the importance of that next to the last slide is not as a basis for design of compliant wall surfaces because it really represents a zero th order calculation. What we have done is calculate the fundamental frequency, the natural frequency of the surface motion. The authors, at least except for our own data, have never attempted to characterize the natural frequency of the surface motion. So what that showed was the first mode vibration frequency as a ratio of the peak frequency in the turbulent boundary layer. We believe that the surface motion has to scale with the flow. We don't believe that the first vibration mode is the mode set up on the surface when we have compliant wall drag reduction. But we believe that the first mode gives an order of magnitude estimate of the natural frequencies that we might encounter on that surface. We intended that figure to show that there appears to be at least a crude correlation between the natural frequency of the surface motion and the characteristic frequencies within the turbulent pressure spectrum. Now that doesn't show the specific frequency of the wall motion. Nobody has measured wall motion for us. We are trying now but we have resolution problems.

We believe that the wall motion, is in an unsteady sense, stabilizing the attached portion of the sub-structure by introducing a coherent periodic pressure fluctuation in the sub-structure. We may in fact stabilize that structure and hold these bursts back from forming until hopefully a favorable pressure gradient comes along and tends to push it back down and accelerate the flow. This is the fluid side; this is the model that we propose. Now we can't prove it, on the structural side we have to drive that surface with something. There are two very interesting points that were made today. First of all on that vibrating cylinder experiment, the frequency of the cylinder turned out to be four times the driving frequency which I think is a very important parameter. I don't quite know how to characterize that. And the other point which was made was that the surface motion can respond to a different portion of the wall pressure spectrum than the peak. Just how this is all incorporated right now we do not know.

Edward Blick, University of Oklahoma: I would like to back up Bob concerning the very small amplitudes in air membrane. I ran some calculations about 7 or 8 years ago and I think we used Willmarth's data for pressure fluctuations in air and I came up with typical numbers like 10^{-4} or 10^{-5} centimeter amplitudes - very, very small amplitudes. You wonder

what these amplitudes could do to the flow, but nevertheless that's what we came up with in our calculation.

Concerning the mechanism for drag reduction, as far as I know, no one knows the answer. Some have speculated and we have done a few calculations, but nothing definite. It looks like it is possible to alter the local Reynolds stress right above the wall if you can get your u and v velocity fluctuating components in phase. Normally the Reynolds stress term is a negative term but if you get your u perturbation and your v perturbation in phase then that is a positive contribution. So it has been speculated that perhaps the oscillation of the wall should be tuned to obtain the u and v perturbations in phase and obtain a positive Reynolds stress, thus reducing the wall shear stress. We have measured turbulent intensity in turbulent boundary layers over the walls in which we thought we were reducing the drag. We observed reductions in the turbulent intensity and the Reynolds stress in these boundary layers above the compliant coating.

Ash: You can show theoretically that a sinusoidal surface motion does in fact produce a reduction in the shear stress. But you can also show, if you are a little bit careful, that the normal stress contribution produced by that same sinusoidal surface motion is nearly twice as large as the reduction in the Reynolds stress and in fact you have an increase in skin friction rather than a decrease so we do not believe at this time that what I thought was a great idea at one time can explain skin friction reduction on a compliant surface.